Engineering Structures 132 (2017) 1–13

Contents lists available at ScienceDirect

Engineering Structures

journal homepage: www.elsevier.com/locate/engstruct

Structural behavior of a new moment-resisting DfD concrete connection

Jianzhuang Xiao [a,b,*], Tao Ding [a,*], Qingtian Zhang [a]

[a] Department of Structural Engineering, Tongji University, Shanghai 200092, China
[b] State Key Lab. for Disaster Reduction in Civil Eng., Tongji University, Shanghai 200092, China

ARTICLE INFO

Article history:
Received 19 November 2015
Revised 6 November 2016
Accepted 8 November 2016

Keywords:
Design for deconstruction (DfD)
Concrete connection
Structural behavior
Moment-resisting
Natural aggregate concrete (NAC)
Recycled aggregate concrete (RAC)

ABSTRACT

Design for deconstruction (DfD) is a burgeoning concept in civil engineering. DfD building components have the possibility to be reused as a second life at the end of the building's first service life. A simple moment-resisting DfD concrete connection for concrete frame joints was proposed in this study. Five full-scale specimens were tested to explore the effectiveness and limitations of the new developed DfD concrete connections. Both static and cyclic flexural loading tests were conducted. Beams made of natural aggregate concrete (NAC) or recycled aggregate concrete (RAC) were extended from column faces. Test results confirmed that the achievement of reinforcement continuity significantly improved the structural behavior of DfD concrete connections. The proposed DfD concrete connections, made of NAC and RAC demonstrated favorable ductility under static and cyclic loadings respectively. In addition, mechanical removal process was easy during the deconstruction stage on account of little post-cast concrete.

1. Introduction

The sustainability of concrete industry is imperative to the global environment and human development. The environmental issues associated with CO_2 emission and construction and demolition (C&D) waste generation of concrete industry play a leading role in the sustainable development of the world [1]. During past several years, techniques on recycling of waste concrete have achieved great progress from mechanical properties of recycled aggregate concrete (RAC) [2–6] to structural performance of RAC structures [7–10]. In addition to waste concrete recycling, reuse of concrete components is also a hot topic among the research area in recent years and has achieved certain progress.

Design for deconstruction (DfD) is a burgeoning concept in civil engineering beyond precast structures [11,12], which initially comes from the field of design for disassembly in mechanical industries [13]. For DfD structures, disassembly building elements have the possibility to be reused as a second life at the end of the building's initial service life. Traditional architectures such as timber structures in ancient China and modern steel frame structures are typical examples of DfD structures. In recent years, methods and tools like life cycle assessment (LCA) and building information modeling (BIM) [14] have been adopted to assess the economic and environmental benefits of DfD applications in civil engineering.

In fact, the DfD concept has been applied to building structures for more than 10 years. In the year around 2000, the CIB (*International Council for Research and Innovation in Building and Construction*) Task Group 39 (Deconstruction) released series reports to state the status of deconstruction in a variety of countries at that time [15,16]. The DfD cases in countries like Australia, Germany, Israel, Japan, Netherlands, Norway, the UK and the US were presented and discussed in these reports. Addis and Schouten [17] and Crowther [18] also defined several principles for DfD applications. According to their suggestions, the connections between structural components are essential and important when applying DfD purpose in civil engineering. That is, the design of connections and connectors of structures should withstand repeated applications.

Generally speaking, it is found that the application of DfD purpose in the case of concrete structures is more challenging than any other types of structures. Due to the requirements of monolithic connections between structural components, abundant cast-in-situ concrete is usually incorporated in the connection area which leads to difficulties in subsequent disassembly. Even so, there are still a number of experimental researches focusing on the concrete components connection to pursue an opportunity of demountability.

From the point view of DfD concrete connections, those dry concrete connections without or with very little cast-in-situ concrete construction, is regarded as suitable for DfD purpose. Some novel connection designs for frame structures, such as dowel connections [19–23], pre-stressed connections [24–27] and

* Corresponding author at: Department of Structural Engineering, Tongji University, Shanghai 200092, China.
E-mail addresses: jzx@tongji.edu.cn (J. Xiao), 1130461@tongji.edu.cn (T. Ding).

http://dx.doi.org/10.1016/j.engstruct.2016.11.019
0141-0296/

hybrid-steel connections [28–32] which possess a certain degree of demountability have been studied in past years. It is found that only low-rise buildings can be designed employing the pinned dowel connections because this kind of connection cannot withstand bending moment during earthquake actions. The prestressed connections and hybrid-steel connections usually exhibit the desired structural performance. The capacity and energy dissipation characteristics of specimens with these connections are adequate compared to monolithic specimens. However, disadvantages such as complicated construction, additional equipment and technology limit the application of these connections. In addition, no intended research directly for DfD concrete connections has yet been found for these types of connections.

Particularly, due to the possible continuity of reinforcements in the joint area and avoidance of the inherent plastic hinging region, beam-to-beam concrete connection is deemed as the best way to pursue DfD purpose for concrete frame structures. Investigators [33,34] found that the beam-to-beam connection is feasible as a replication of cast-in-situ concrete moment-resisting frames, as the crack propagate, failure pattern and the ductile behavior performs similarly. In addition, the frame with beam-to-beam connection allows the formation of plastic hinges located at the beam-end regions. However, for the purpose of DfD, only one pioneer research was found to verify the structural behavior of beam-to-beam concrete connections after deconstruction and reconstruction [35]. They proposed a DfD moment-resisting beam-to-beam connection for application in typical multi-storey reinforced concrete (RC) apartment blocks. For this type of beam-to-beam connection, the bolted end plate steel connection was selected as the basis for the proposed DfD moment-resisting connection. However, it was stated by their own investigations that mechanical demolition work during deconstruction may damage the connection resulting in much clamor and debris.

As a result, to the best knowledge of the authors, the amount of performed tests on the structural behavior of DfD concrete connection is still insufficient. It is well known that, for long span frame structures, the structural behavior of the frame system is expected to be governed by flexure rather than by shear. It is important that DfD concrete connection can transfer the flexure which is externally applied through the beams to the columns. Therefore, the present study proposes a moment-resisting DfD concrete connection by welding the steel at both ends of the reinforced concrete beam. Experiments were carried out to evaluate the structural behavior and demountable flexibility of DfD ductile connections proposed in this study. A total of five full-scale concrete specimens were designed and tested to failure under both static and cyclic flexural loadings.

2. Experimental program

2.1. Design and details of specimens

Reuse flexibility is the major issue that needs to be addressed for DfD structures. The layout of the original building is very likely to differ from the new one. As a result, the DfD specimen in this study was mainly focused on beam components. Moreover, in order to avoid complicated construction process and high economic cost, the welding method was adopted for the proposed DfD ductile connection in this study. Fig. 1 shows the prototype of the DfD concrete frame system and Fig. 2 displays the details of the proposed DfD concrete beam to be tested in this study. The construction detail consisted of a middle precast beam, which was placed on a short protruding beam. The short protruding beam was extended from the column of a frame structure. More importantly, by moving the connections away from the column face, the coinciding condition between the inherent plastic hinge locations and the connection regions could be avoided. It is expected that this arrangement will greatly enhance the structural safety of the proposed DfD system.

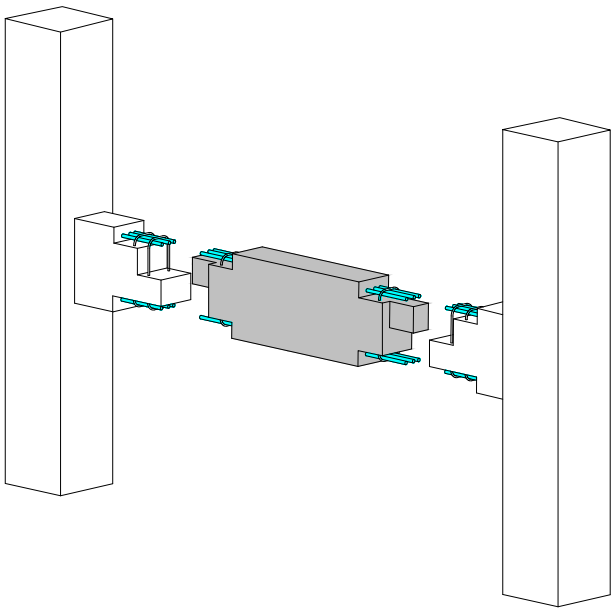

Fig. 1. Prototype of the DfD concrete structure.

Within the connection region, the main reinforcements in both the top and bottom of the beam were welded to the main reinforcements of the frame columns. Elaborate design on the position and dimension of the steel should be carefully taken into account to provide feasible connection assembly on-site in the future. Once the middle precast beam was located on the column and reinforcement connection was achieved, only a very small amount of cast-in-situ concrete was placed for the convenience in future deconstruction. The post cast-in-situ concrete only provided the compression stress transfer and played a role in providing protection for steel bars against possible corrosion and fire during their service life.

During the deconstruction process, the post cast-in-situ concrete was dismantled and the welding reinforcement was cut off by mechanical tools. It is predictable that only minimal damage would be brought due to the small quantity of post cast-in-situ concrete. Conceptually, with proper reinforcement design of new frame columns, the middle beam can be reused as a second life, achieving the DfD purpose and the sustainability.

In order to obtain a comprehensive understanding on the structural behavior of the proposed DfD concrete connections, both static and cyclic flexural loadings were applied to the specimens in this study. In consideration of possibilities that RAC could also be applied for sustainable purpose, specimens made of RAC were also casted and evaluated.

During the static loading tests, three specimens were completed and studied. They were monolithic natural aggregate concrete (NAC) specimen (MNS), DfD NAC specimen (DNS) and DfD RAC specimen (DRS-1). Specimen MNS was designed as a reference specimen. It did not contain any DfD connection. Specimen DNS was designed and constructed with a DfD ductile connection which was proposed in this study. For specimen DRS-1, the reinforcement and design method was a replication of DNS except for casting with RAC. For the sake of reflecting the behavior under earthquake actions, another two specimens including monolithic RAC specimen (MRS) and DfD RAC specimen (DRS-2) were tested under the cyclic loading. Specimen MRS was taken as a reference

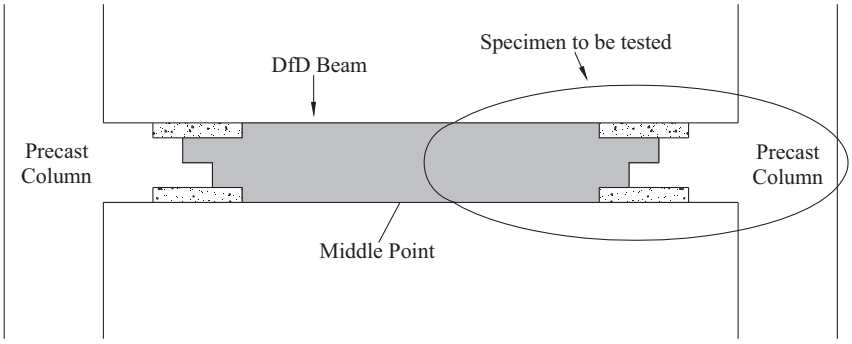

(a) Specimen to be tested in this study

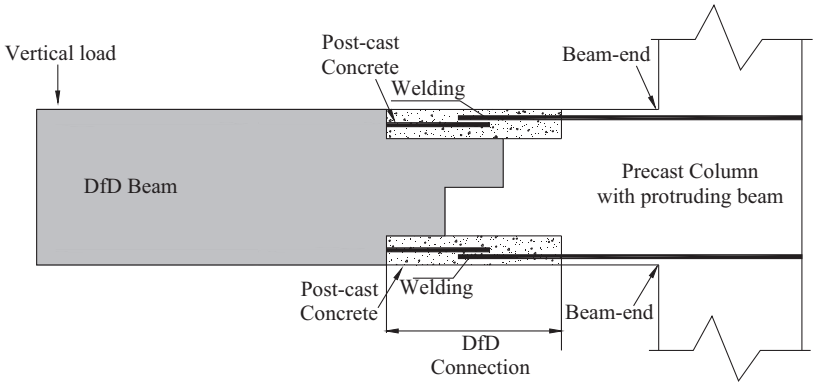

(b) Elevation view of the connection in details

Fig. 2. Details of the proposed DfD concrete connection tested in this study.

specimen and specimen DRS-2 was a replication of DRS-1. Variables of the five full-scale test specimens are summarized and listed in Table 1.

Since the main purpose of this study was to verify the structural behavior of DfD connection on the concrete frame beam, the beam was extended from a column which was much stronger than the tested beam.

Details of the geometrical dimensions and reinforcement arranged in the five test specimens are illustrated in Fig. 3. The lengths of each region were kept constant in all specimens so that to make a comparison. All DfD connection specimens had the same geometrical dimensions of the protruding beam and same arrangements of the welding reinforcement in the post-cast area. The section of the beam was 200 mm × 400 mm. The total length of all the beams was 1600 mm. For DfD specimens, the length of middle precast beam and protruding beam were 1200 mm and 515 mm, respectively. The connection specimens were designed according to the "strong column-weak beam" design criterion and had the same geometrical dimensions. The section of column is 650 mm × 650 mm and eight 25-mm diameter bars were employed for the reinforcement of columns which ensures that the moment resistance of column was twice of the beam. Beams were reinforced using three 16-mm diameter bars both at the bottom and at the top. For the monolithic specimens, beam bars were made continuous through the entire span. While for the DfD specimens, welding bars were used at the top and bottom to connect two parts of the component. In the connection area, transverse reinforcement of the beams, required for shear resistance and concrete confinement was provided. In addition, 12-mm or 14-mm rebars was employed in this area, seen in Fig. 3(d). This is the major reinforcement difference between monolithic and DfD specimens.

2.2. Material properties

With an appropriate mix design, it is believed that RAC can be proportioned to have the same strength properties to that of NAC. Several mixture proportioning methods, such as equivalent mortar volume approach [36] and two-stage mixing approach [37,38], have been proposed to allow one to determine the proper amount of RCA and other mix ingredients to achieve certain

Table 1
Variables of test specimens.

Specimen no.	Specimen	Concrete type	Monolithic or demountable	Loading method	Remarks
1	MNS	NAC	Monolithic	Static	Reference specimen
2	DNS	NAC	Demountable	Static	
3	DRS-1	RAC	Demountable	Static	
4	MRS	RAC	Monolithic	Cyclic	Reference specimen
5	DRS-2	RAC	Demountable	Cyclic	

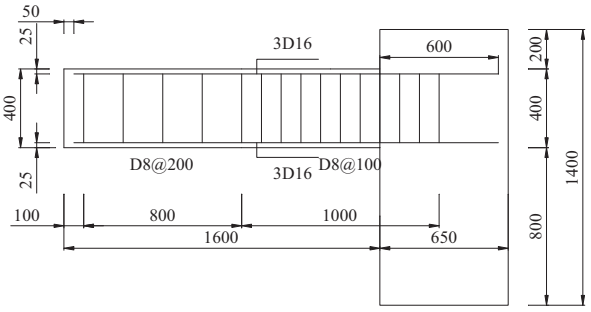

(a) Elevation view of reference monolithic specimens

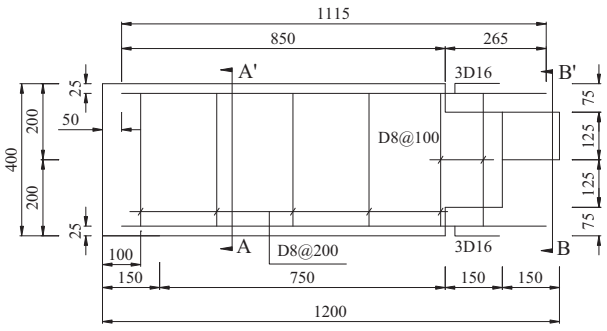

(b) Elevation view of the left part of DfD specimens

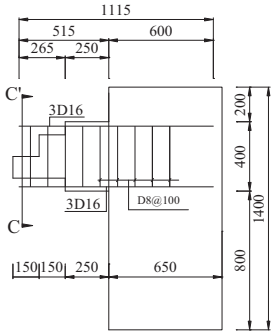

(c) Elevation view of the right part of DfD specimens

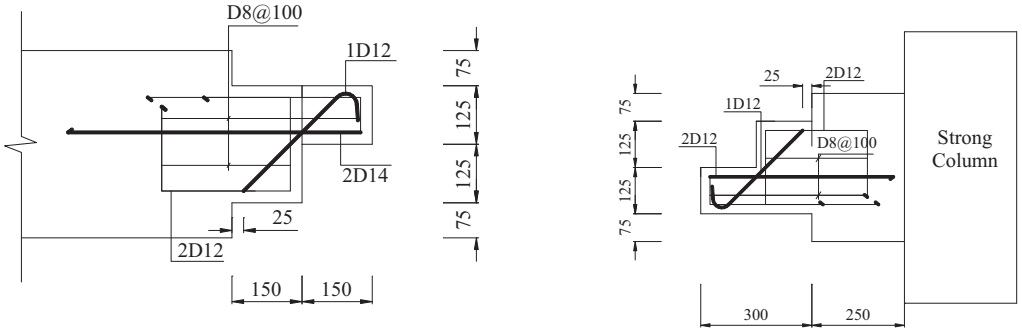

(d) Reinforcement of protruding beams

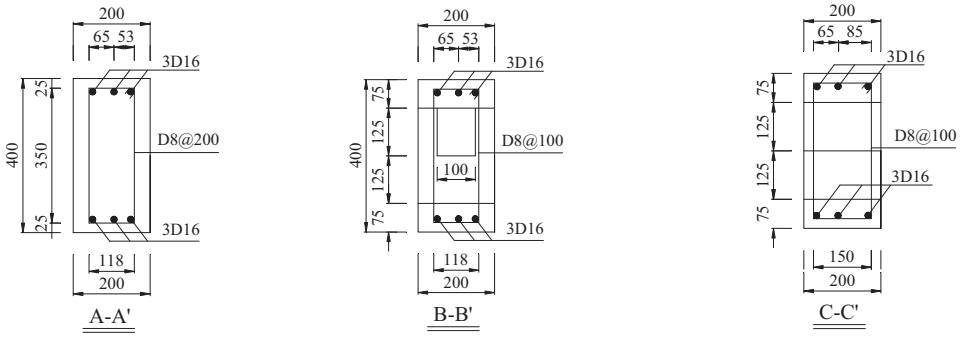

(e) Reinforcement of sections

Fig. 3. Dimension and reinforcement details of specimens.

specified concrete strength. In order to investigate the effect of RAC, NAC and RAC were designed with a similar target compressive strength. The concrete's cube compressive strength of all the test specimens was designed to be 30 MPa. The strength grade of post-cast concrete was also targeted to be 30 MPa, which is considered to prevent corrosion, fire attack for steel bars and provide compression stress transfer. Ordinary Portland cement, river sand and natural coarse aggregates (NCA) with size ranging from 5 mm to 25 mm were used for the concrete mix in this study whereas Recycled coarse aggregates (RCA) with the same size range were produced after crushing and sieving of waste concrete from a demolished concrete structure. Table 2 presents the basic properties of RCA and NCA. For RCA, the gradation was similar to that of NCA adopted in this study. The detailed mix proportions

Table 2
Basic properties of recycled coarse aggregate and natural coarse aggregate.

Properties	Recycled coarse aggregate (RCA)	Natural coarse aggregate (NCA)
Content of attached old mortar	33%	0%
Loose packing density (kg/m^3)	1280	1360
Tight packing density (kg/m^3)	1440	1480
Apparent density (kg/m^3)	2530	2660
Crushing value index	11%	5.1%
Clay content	1.8%	0.8%
Water absorption	3.5%	1.0%

with a slump of 200 mm are listed in Table 3. It can be inferred from the two tables that appropriate decrease of water to cement ratio should be reminded in RAC mix proportion, due to the relative inferior properties of RCA.

Cubes of 150 mm length were cast and cured simultaneously with specimens to determine the compressive strength of the concrete. The compressive strength obtained from the testing of concrete specimens is also given in Table 3. Table 4 presents the mechanical properties of the steel used in this study, including the average yield strength and elastic modulus.

2.3. Test procedure

As stated above, two-stage test program was conducted during this study. Firstly, specimens of MNS, DNS and DRS-1 were tested under static loading in order to obtain essential information on the structural behavior of the proposed DfD ductile connections. Based on the information from the static loading tests, the rest two specimens MRS and DRS-2 were then tested under low frequency cyclic loading in order to acquire necessary structural behavior of DfD specimens made of RAC under earthquake actions. The cyclic loading process included two main steps, namely a load control step and a displacement control step. Fig. 4 shows the test set-up for the static loading and low frequency cyclic loading. Fig. 5(a) is a picture showing the specimen before the test. During the test, the load was applied vertically with this set-up on specimens.

The measurements throughout the tests were the deflection and rotations of the beam, deformation and the rotation of the column. The arrangement of Linear Variable Differential Transducers (LVDTs) is shown in Fig. 5(b). The vertical displacements along the specimen length were monitored and recorded based on these LVDTs. The ratio of vertical displacement to the length could reflect the rotation of the beam. Two LVDTs were used to record the deflection of the beam including the displacement of the beam and displacement at the connection part. Additionally, three LVDTs were used to monitor the displacement of the strong column. Furthermore, in order to track the different strain history among the specimens, strain gauges S1-S6 were mounted onto the longitudinal reinforcement and six strain gauges were attached on the surface of the concrete. Fig. 5(b) also shows the layout of steel strain gauges on the top and bottom longitudinal bars in the beam.

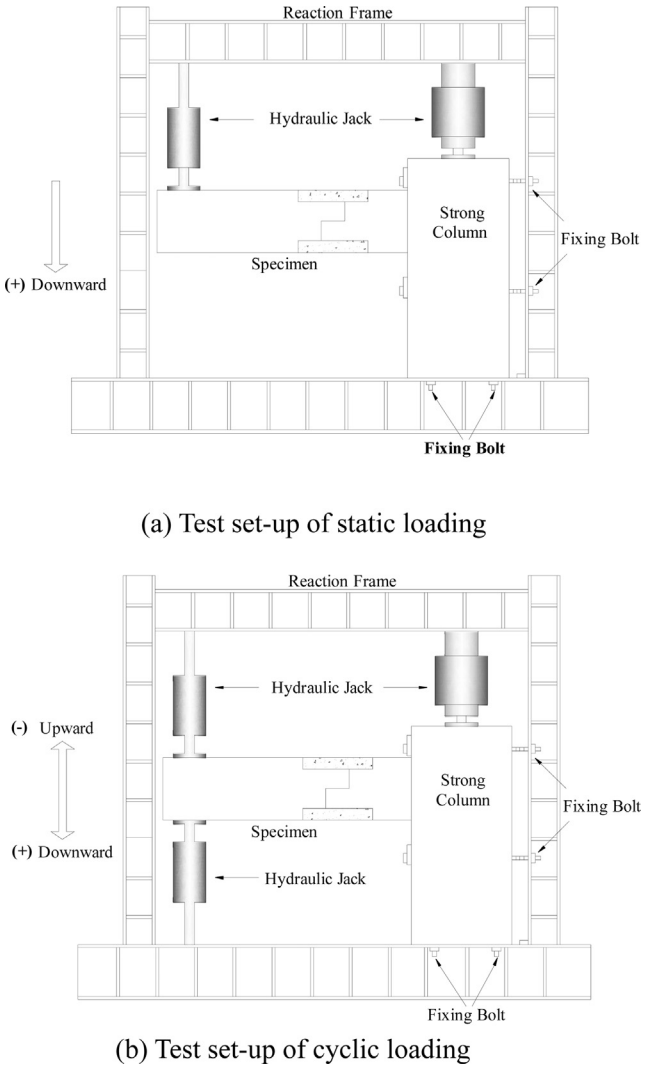

Fig. 4. Test set-up.

3. Test results

3.1. Crack propagation and failure patterns

The crack propagation of the five specimens throughout the tests is drawn in Fig. 6. Details of the crack propagation of the five specimens are described in the following:

Table 3
Mix proportions of concrete and compressive strength of concrete (1 m^3).

Concrete type	w/c ratio	Water (kg)	Additional water (kg)	Cement (kg)	RCA (kg)	NCA (kg)	Sand (kg)	Compressive strength (MPa)
NAC	0.45	160	0	356	0	1080	684	42.6
RAC	0.42	160	10.8	381	1024	0	740	42.0

Table 4
Mechanical properties of the steel.

Steel type	HRB300 D8	HRB400 D12	HRB400 D14	HRB400 D16
Yield Strength (MPa)	396	517	490	456
Elastic Modulus (GPa)	211	191	198	195

(a) Specimen on the reaction frame before tests

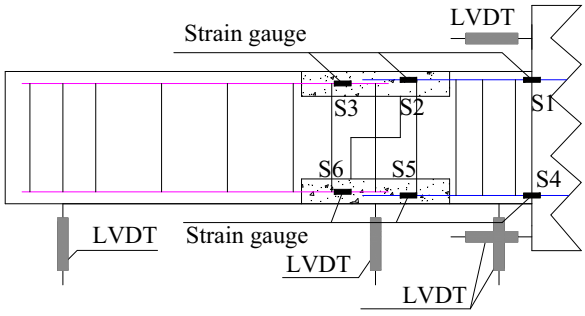

(b) Schematic illustration and numbering of instruments

Fig. 5. Instrumentation of tests.

3.1.1. Specimen MNS (reference specimen under static loading)

Under static loading, the first flexural crack generally occurred along the beam-end of the monolithic specimen. Location of beam-end described in this study could be found and described in Fig. 2(b). With the increase in applied loading, a wide range of fine vertical cracks formed and propagated downwards. Particularly, cracks were located at the end of the specimen and distributed in a range of length equal to the beam height, crack width was larger and developed faster. It was also observed that many fine cracks stopped developing in a certain degree. However, there were mainly three diagonal cracks with about 45 degree angle developed directing to the bottom of beam-end. After the yielding load applied on the specimen, only the main vertical and diagonal cracks gradually widened. Specimen failed in flexure with crushing of the compression concrete at the maximum moment zone after the main reinforcement being yielded.

3.1.2. Specimen DNS (under static loading)

Under static loading, the first flexural crack appeared along the beam-end of the DfD specimen, which was similar to the monolithic specimen. Fine vertical cracks also occurred at the top of beam-end downwards with the increase of applied loading. It was fortunately observed from the test that most of these flexural cracks and main diagonal cracks were formed at the protruding beam, which met with the initial design purpose. The first vertical cracks in the DfD specimens initiated close to the post-cast concrete region. This behavior can be mainly attributed to the discontinuity of concrete in the post-cast concrete region of the DfD specimens. However, with the drift increase, the flexural cracks penetrated from the post-cast region to the reusable beam part, indicating a good integrity of the DfD connection as a whole. It is believed that the continuity of longitudinal reinforcement played an important role in increasing the integrity of these DfD specimens. When the specimen was subjected to the ultimate load, it failed in flexure with crushing of the compression concrete at the maximum moment zone. In addition, only a few cracks can be found on the DfD part before the yielding load.

3.1.3. Specimen DRS-1 (under static loading)

Serving as the DfD specimen using RAC, no significant difference on crack propagation was observed on DRS-1 during the test. The first flexural crack also appeared along the interface between cast-in-situ concrete and precast concrete. After that, fine flexural cracks occurred on the top of beam-end for the DfD RAC specimen under static loading cracking. It was observed that the cracks' formation of DRS-1 showed a similar process compared to DNS. Even though, some major distinction can also be observed. Relatively speaking, more cracks appeared on specimen DRS-1 than DNS, especially in the connection area, where the concrete was post-cast. This phenomenon may mainly attribute to the construction quality and unique structural behavior of RAC [4]. However, no obvious damage cracks can be found on the DfD part and the specimen still failed in flexure due to the crushing of the compression concrete at the beam-end.

3.1.4. Specimen MRS (reference specimen under cyclic loading)

Under cyclic loading, the first flexural cracking load was lower than the data recorded in static loading. With the increase in loading, the rate of crack development slowed down. When the load imposed was around 60 kN, the cracks propagated and extended rapidly due to the longitudinal reinforcement reaching its yield strength. Shear cracks also became apparent when the test progressed into the elastic-plastic stage and kept propagating in a diagonal direction toward column faces. After the yielding point, although the loading increased slowly, both length and width of the cracks developed quickly accompanied with an increasing deflection of the beam. At last, concrete at the beam-end was crushed due to compression and test ended in a typical pattern of flexural failure.

3.1.5. Specimen DRS-2 (under cyclic loading)

Under cyclic loading for the DfD specimen made of RAC, the first flexural crack also formed along interface between cast-in-situ concrete and precast concrete. In addition, the crack propagation was almost the same compared to specimen MRS. However, some useful observation can also be recognized. On the protruding beam, both the vertical and diagonal cracks shaped and presented in a symmetrical pattern. At the end of specimen, the vertical cracks crossed first and then the diagonal cracks followed. A "V" pattern of diagonal cracks can be found on the protruding beam of the DfD specimen, as shown in Fig. 6(e). This area can be regarded as the plastic hinge zone for the specimen under earthquake actions. The test result is consistent with the initial design purpose and proves that the DfD RAC specimen has favorable integrality. It is interesting to find that flexural cracks across the area between the new and old concrete. Fortunately, at the end of the test, concrete at the beam-end was also crushed due to compression and test ended in a typical pattern of flexural failure as well.

3.1.6. Comparisons

It can be inferred from the test results that all these specimens were not experienced a shear failure until the end of tests. As a whole, the crack propagation on the frame beams was found to be different among these specimens.

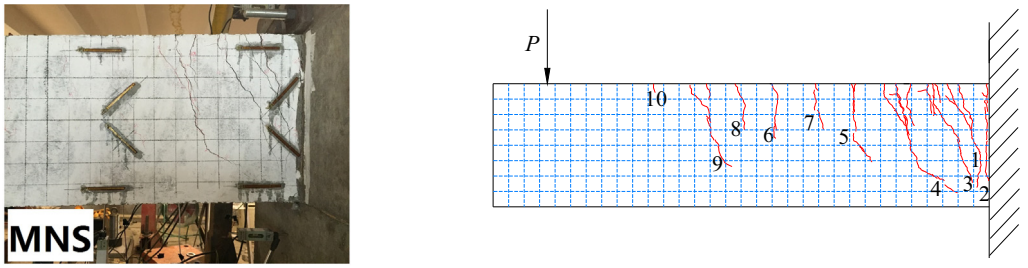

(a) Specimen MNS

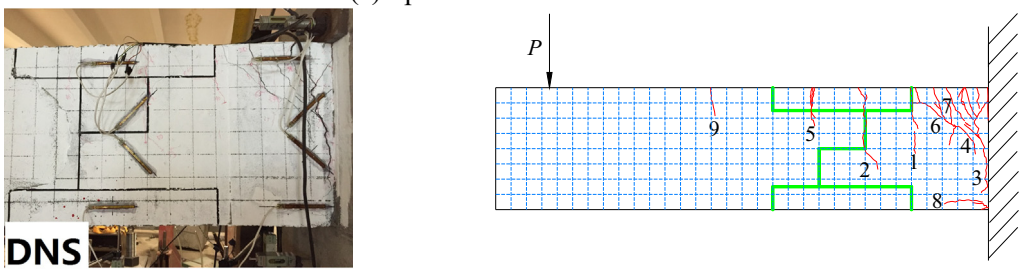

(b) Specimen DNS

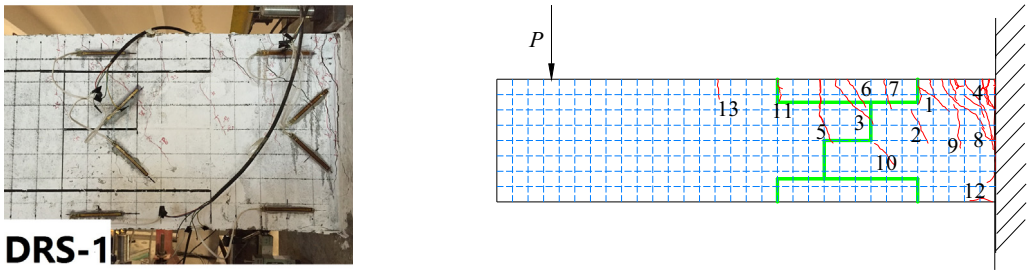

(c) Specimen DRS-1

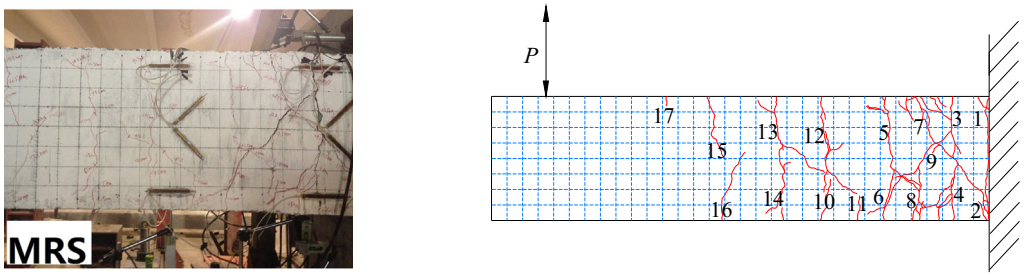

(d) Specimen MRS

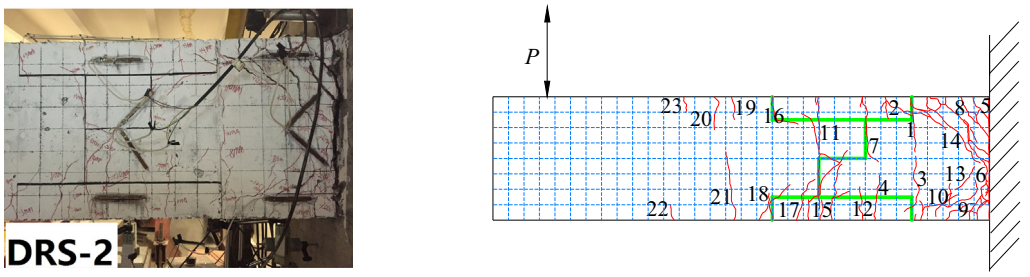

(e) Specimen DRS-2

Fig. 6. Crack patterns of specimens.

It was found that the beam cracking distribution for MNS and MRS was very uniform, with approximately 100 mm spacing. However, compared to these two specimens, the cracking distribution for specimen DNS, DRS-1 and DRS-2 shows significant differences. Due to the stiffness mutation and stress concentration at the interface between cast-in-place concrete and post-cast concrete, the first flexural crack was always found to be formed along interface between the two concrete parts. Furthermore, at the post-cast concrete region, about 50% more cracks were propagated along the horizontal and vertical interface between the old and new concrete compared to the monolithic specimens.

In general, for the monolithic specimens, at the final stage of loading, severe spalling of large pieces of cover concrete was observed at the fixed end of the beam. Compared to the monolithic specimens, it is found out from test results that more concrete spalling happened at the beam-to-beam connection area on DfD specimens.

3.2. Stress behavior

In order to keep the capacity of the DfD connections as same as that of monolithic structures, the initial design purpose was to make the plastic hinge located at the short protruding beams. Thus, Fig. 7 shows the strain measurements obtained from strain gauges for specimens under static loading. It was displayed to investigate whether the strain discontinuity between the components would occur at the proposed DfD concrete connection. The strain gauges were attached on the longitudinal reinforcement at the beam-ends and connection areas. Locations of the attached strain gauges S1-S6 are presented in Fig. 3(c).

As shown in Fig. 7, the strain values from the six strain gauges increased proportionally with the increase of the applied load for all the three specimens, and no abrupt variation of the strain was observed until the failure of the specimens. The strain distribution of the monolithic specimen was almost identical to the DfD specimens. This trend indicates that these specimens successfully sustained the applied loads. Therefore, the load transfer integrity of the proposed DfD concrete connection system is secured, and the stress distribution can be predicted appropriately by the elasticity theory.

On the other hand, the strains of the longitudinal tension reinforcement located at S2 and S3 of DfD specimens were somewhat higher than that of monolithic specimen. This phenomenon demonstrates that, under the same applied load, the deformation of connection area for the DfD specimens was relative larger. And the shear deformation in the DfD specimens was larger than that in the monolithic specimens. It is believed that the welding quality and the extra transition zones between discontinuous concrete elements would influence the strain distribution of the DfD specimens.

The strain gauges attached on concrete were used as auxiliary verification on strain behavior. For the local behaviors of the concrete, no matter the monolithic specimen or the DfD specimen, the measured strain at the end of the beam was always somewhat larger than the data recorded from the connection part. For example, for monolithic specimen MNS when the first crack appeared, the measured strain was 174 με at the end of the beam and 123 με at connection part. For DfD specimen DNS at this stage, the measured strain was 259 με at the end of the beam and 74 με at connection part. These results agreed well with the observation that more cracks appeared at the end of the beam than connection part due to vertical loadings.

3.3. Load and deflection

From the records of LVDTs, it is verified that the deformation and the rotation of the column were very small. The beam and connection deflections of three specimens against the total applied static load are plotted in Fig. 8. It is inferred from Fig. 8 that the yielding loads of the three specimens were almost identical. The load applied on specimens MNS, DNS and DRS-1 approximately remained consistent before the yielding of the longitudinal tension reinforcement. After the level of yielding load, the deflection of three specimens sharply increased with the occurrence of the increasing flexural cracking, which is in agreement with the typical flexural behavior of reinforced concrete beams [32].

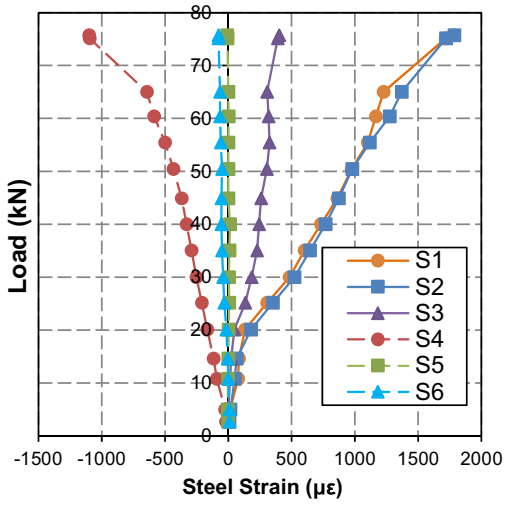

(a) Specimen MNS

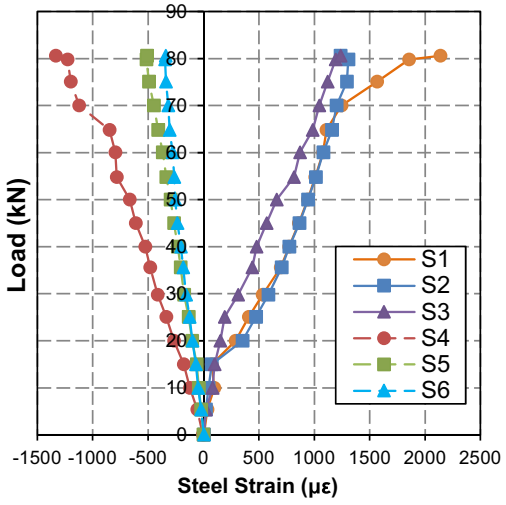

(b) Specimen DNS

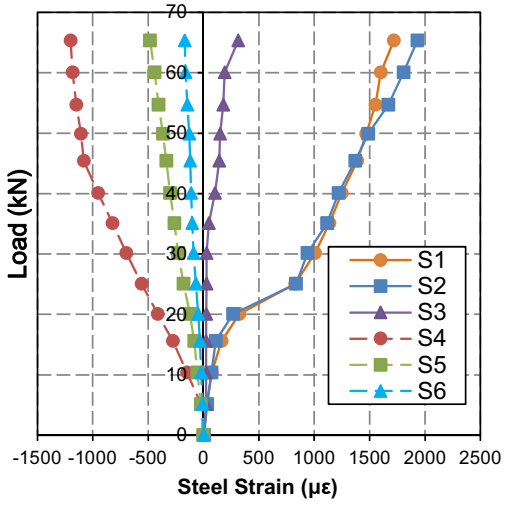

(c) Specimen DRS-1

Fig. 7. Strain behavior of longitudinal reinforcement under static loading.

In general, the differences about load and deflection behavior among these beams subject to static loading were very small. However, some interesting phenomenon can still be found from Fig. 8.

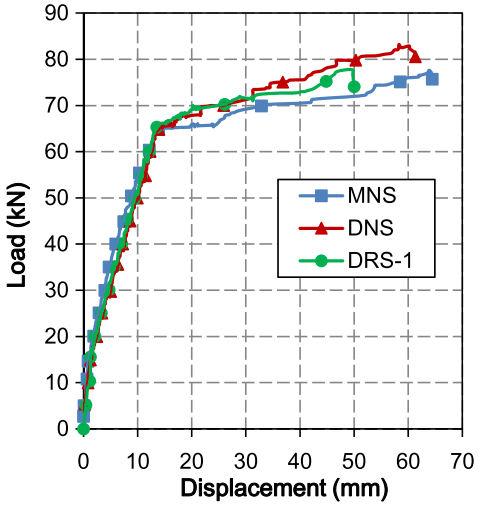

(a) Load versus displacement of the beam

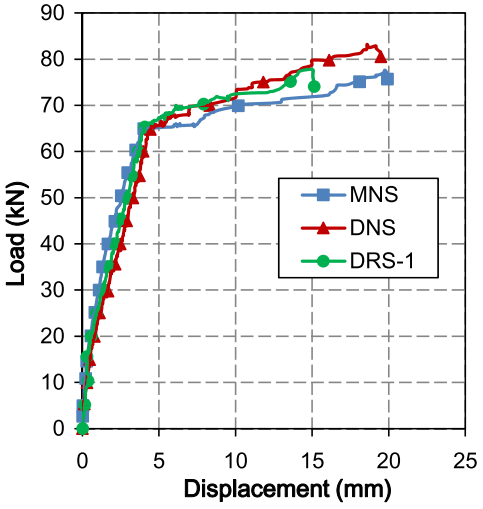

(b) Load versus displacement at DfD connection

Fig. 8. Load versus deflection curves under static loading.

The initial flexural crack load of specimen MNS was respectively higher than those of specimen DNS and DRS-1 by 33% and by 18% respectively, but with a relative lower ultimate load. The lower cracking load of DfD specimens may be due to the extra transition zones between discontinuous concrete components for DfD purpose. However, as seen in Fig. 3(c), due to the sufficient reinforcement of the protruding beam, the ultimate load of DfD specimens DNS and DRS-1 can even be higher than that of monolithic specimen MNS. Results from this test demonstrate that DfD purpose did not influence the loading capacity of specimens. It is also noticed that specimen DRS-1 made with full RAC should be assessed a bit inferior from the structural behavior point of view, taking into account of the ultimate displacement. The results show that the employment of RAC has slight influence on the behavior of beam with the same reinforcements and design procedures. The test results presented here are also in accordance with previous studies which were mainly focused on monolithic RAC beams [39,40].

In addition, Fig. 9 shows the beam deflection against the connection deflection during the whole tests. The tangent slope can be seen as the ratio of beam deflection to the connection deflection. Obviously, curves in Fig. 9 keep straight lines until the failure of

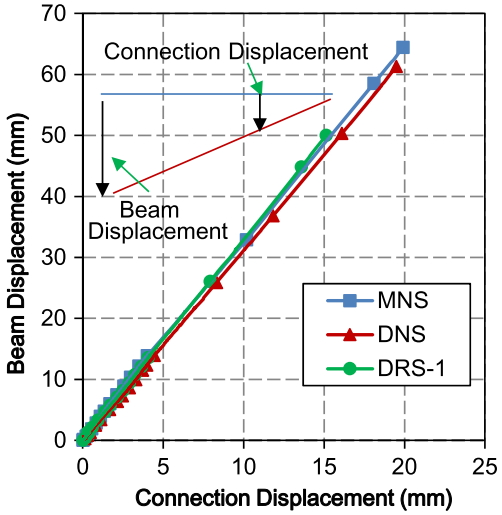

Fig. 9. Relationship between beam displacement and DfD connection displacement.

specimens, which means that no abrupt displacement variation was occurred during the whole test process in either of the monolithic and DfD specimens. This result was identical to the previous analysis on the steel stress, indicating that the load transfer integrity of the proposed DfD concrete connection system is favorable.

3.4. Hysteretic loops and skeleton curves

Fig. 10 shows the hysteretic curves of specimens MRS and DRS-2, which trace the development of vertical displacement of the beam under low frequency cyclic loading. Obviously, the two hysteresis curves show no obvious difference and have a fine shape from the seismic behavior point of view. When the applied load was less than about 30% of the maximum load, i.e., at the stage of no cracking or just before cracking, the hysteretic curves of the two specimens were approximately straight lines. Within each cycle, the decrease of the secant stiffness caused by the cyclic loading was somewhat insignificant and the residual displacement was very small. When the specimen stepped into an elastic-plastic range, degradation occurred in both the load capacity and the rigidity, which reflected the damage accumulation in the specimen. During the whole process of the cyclic loading tests, no significant effect is observed on the hysteretic curves between monolithic and DfD specimens.

According to the hysteretic curves, Fig. 11 shows the load versus vertical displacement skeleton curves of the two specimens. From the skeleton curves, the cracking load point, the yield load point, as well as the ultimate load point can be easily recognized. Two important findings can be inferred from the skeleton curves shown in Fig. 11. Firstly, the initial stiffness of the two specimens was similar regardless of monolithic or DfD specimen before the yielding of specimens. This phenomenon is agreed well with the results from static loading test. The DfD purpose showed some influences on the skeleton curves after the yielding of the specimen. The ultimate capacity of DfD specimen was some larger than the monolithic specimen. As stated previously, this is due to the sufficient reinforcements in protruding beams for DfD specimen. Another important finding from the skeleton curves is that, the capacity and structural behavior of the proposed DfD specimen at both sides were almost the same. This superiority can be attributed to the beneficial effect of stronger connection by steel welding in the connection areas. It confirms that the DfD specimen proposed in this study can well resist the cyclic loading under earthquake actions.

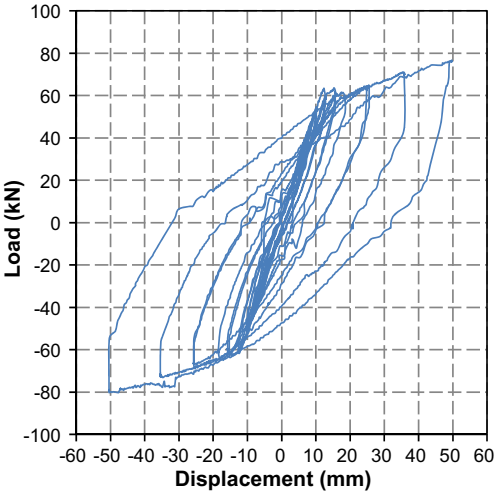

(a) Specimen MRS

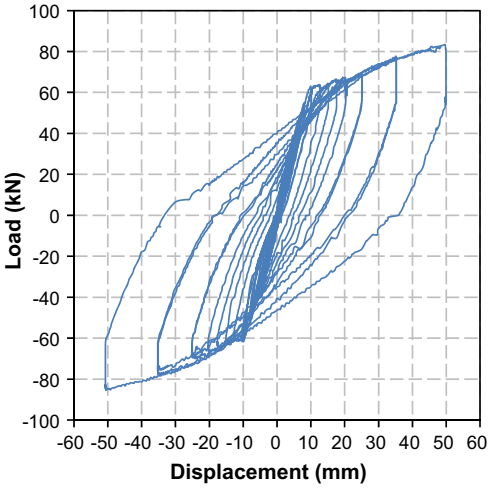

(b) Specimen DRS-2

Fig. 10. Hysteretic curves of specimens under cyclic loading.

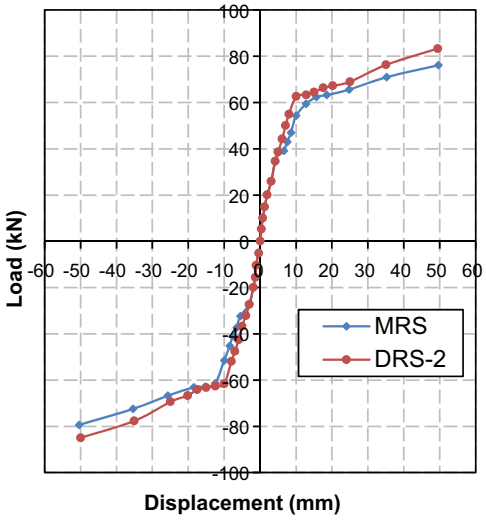

Fig. 11. Skeleton curves of specimens under cyclic loading.

3.5. Characteristic points and ductility ratios

Table 5 summarizes characteristic points including the measured cracking load and displacement, yield load and displacement, as well as the ultimate load and displacement for all the five specimens. It is noted from this table that the crack features and yield features are almost the same for all the specimens. The ultimate features in Table 5 confirm the explanation in Sections 3.3 and 3.4.

The ductility of flexural members is generally evaluated using a displacement ductility ratio defined below [41]:

$$\mu = \frac{\Delta_u}{\Delta_y} \tag{1}$$

where Δ_y is the displacement of the beam at the yielding of the longitudinal tension reinforcement, and Δ_u is the displacement at the ultimate loading of the beam. The ductility ratios obtained from Eq. (1) for the beam specimens are also presented in Table 5.

From the data listed in Table 5, it is clear that the ductility ratio μ value ranges from 3.68 to 4.64 which means all the test specimens showed favorable deformation performance. It is also noticed that the ductility ratio of specimen MNS was the highest, indicating that monolithic specimen made of NAC still has the best structural behavior. In addition, the ductility ratio of specimen DNS was slightly lower than that of specimen MNS, with a decrease about 5.2%. It indicates that the extra transition zones between discontinuous concrete elements have some influence on DfD specimens. However, it is interesting that the influence on the ductility ratio of RAC employment is larger than that of DfD application, as ductility ratios of both the monolithic and DfD RAC specimen are smaller than the specimen DNS. These interesting results prove that, for the ductility of DfD specimens, the property of concrete is still a most important factor compared to the influence of DfD employment. This conclusion meets the original design concept.

3.6. Stiffness deterioration

Under low frequency cyclic vertical loading condition, the stiffness decreased as the drift increased after the yielding of specimens. The ratio of the applied vertical load to the displacement of the beam is denoted as the secant stiffness. It is employed to analyze the stiffness degradation in this investigation. Fig. 12 shows the degradation of secant stiffness versus the vertical displacement of specimens MRS and DRS-2 under successive cyclic loadings. It can be seen from Fig. 12 that the stiffness deterioration of specimen with DfD connection was similar to that of monolithic specimens. The stiffness of two specimens decreased dramatically at the beginning stage of the loading. When cracks appeared, the stiffness reduced to less than 50% of its initial value. After the specimens behaved nonlinearly, the rate of rigidity degeneration slowed down and no abrupt changes were observed during the whole test for the both specimens. Generally, the stiffness degradation of DfD specimen was relative faster than monolithic specimen. However, on the whole, the application of DfD has only nominal influence on the law of rigidity degradation.

3.7. Energy dissipation

The energy dissipation is determined according to the area enclosed by the overall hysteresis of the loading cycle, which is commonly used to quantify the energy absorption ability of RC components or structures. Fig. 13 shows the energy dissipations versus the vertical displacement of the specimens. Generally, the energy dissipation of the two specimens increased with the increasing vertical displacement. DfD specimens are able to sustain

Table 5
Summary of test results.

Specimen	P_{cr} (kN)	Δ_{cr} (mm)	P_y (kN)	Δ_y (mm)	P_u (kN)	Δ_u (mm)	μ
MNS	20.00	1.91	65.00	13.89	75.72	64.45	4.64
DNS	15.00	1.65	64.81	13.93	80.58	61.32	4.40
DRS-1	17.00	1.55	63.33	12.77	74.09	50.00	3.91
MRS	15.00	1.88	63.38	12.87	76.13	49.65	3.86
DRS-2	15.00	1.31	62.59	13.03	83.31	49.45	3.80

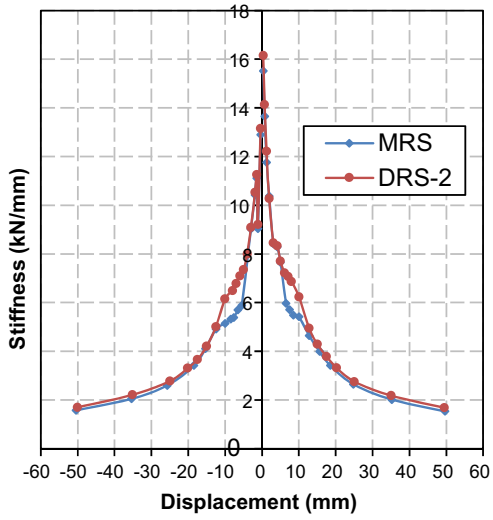

Fig. 12. Stiffness degeneration of specimens under cyclic loading.

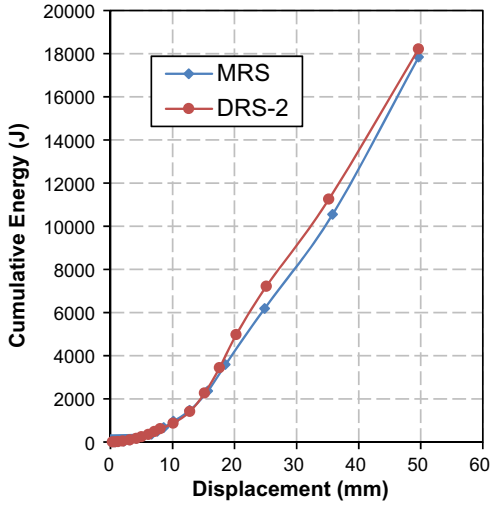

Fig. 13. Energy dissipation of specimens under cyclic loading.

larger energy dissipation capacity when large horizontal drift ratio is achieved. It can also be inferred from Fig. 13 that the energy dissipation of both specimens can be divided into two phases, i.e., pre-cracking phase and post-cracking phase. In the pre-cracking phase, the energy dissipation capacity was very small. When cracks appeared, it was less than 5% of the maximum energy dissipation. No noticeable difference on the energy dissipation capacity can be found even after the cracks appeared. It is known that for RC components, in the post-cracking phase, the energy dissipation relies much more on the openings and closings of cracks on the specimens. Thus, this result confirmed the observation that the crack development of the two specimens was almost identical during the test process. Furthermore, at a same drift ratio, the dissipated energy of DRS-2 was slightly larger than that of the monolithic specimen MRS. This is because that a relative larger bearing capacity was achieved for the reused joint specimens due to the higher concrete strength. This indicates that energy dissipation capacity of beam-column connection is less affected by the proposed DfD method compared to concrete strength.

4. Verification of flexural capacity

ACI 318-08 [42] recommends that the cracking moment M_{cr} and ultimate moment M_u of flexural components can be computed by the following forms:

$$M_{cr} = \frac{f_r I_{g,t}}{y_t} \tag{2}$$

$$M_u = (A_s - A_s')f_y \times \left(d - \frac{a}{2}\right) + A_s' f_y (d - d') \tag{3}$$

where f_r is the strength of fracture, $I_{g,t}$ is the moment of inertia of the gross transformed section; y_t is the centroidal axis depth of the gross transformed section; A_s and A_s' are the area of the longitudinal tensile and compression reinforcements, respectively; f_y is the yield strength of the steel; a is the depth of the equivalent rectangular stress; d is the effective depth of section and d' is the distance between center of compression reinforcement and compression edge of the section.

Flexural capacity recorded from the test results and calculated by equations based on ACI 318-08 is given in Table 6.

The initial cracking moments calculated from ACI 318-08 equations are in good agreement with the test results. The maximum moment capacity predicted from ACI 318-08 equations is somewhat lower for all beams. The ratio of tested moment to the calculated moment M_u^t/M_u^c listed in Table 6 is around 1.4. Therefore, according to the verification by the ACI 318-08 specification and test results, the flexural capacity of the proposed DfD concrete beam made of both NAC and RAC can be safely satisfied.

5. Discussion

In order to assess the reuse flexibility of the proposed DfD system, deconstruction of the DfD specimens were also conducted after the test. The first step was stripping the small portion of the encasing post-cast-in-place concrete away. Mechanical jackhammers could be adopted. For sake of exposing the reinforcement, the deconstruction was executed carefully to ensure as minimal damage as possible. The typical deconstruction process and concrete surface are illustrated in Fig. 14. Once the encased concrete was moved away, the welded steel was fully exposed. Then steel was easy to cut off and the specimen was separated into two segments. During the execution of deconstruction process, mechanical removal process was not so difficult and very little debris was generated. Little damage was occurred on the DfD part and it was easy to conduct the demolishing work.

Table 6
Verifications of test results and calculations.

Specimen	Experiment (kN·m)		ACI 318-08 (kN·m)		Experiment/calculation	
	M_{cr}^{t}	M_{u}^{t}	M_{cr}^{c}	M_{u}^{c}	M_{cr}^{t}/M_{cr}^{c}	M_{u}^{t}/M_{u}^{c}
MNS	28.50	107.90	23.50	80.55	1.21	1.33
DNS	21.38	114.82	23.50	80.55	0.91	1.42
DRS-1	24.23	105.57	23.50	80.55	1.03	1.31
MRS	21.38	108.48	23.50	80.55	0.91	1.34
DRS-2	21.38	118.71	23.50	80.55	0.91	1.47

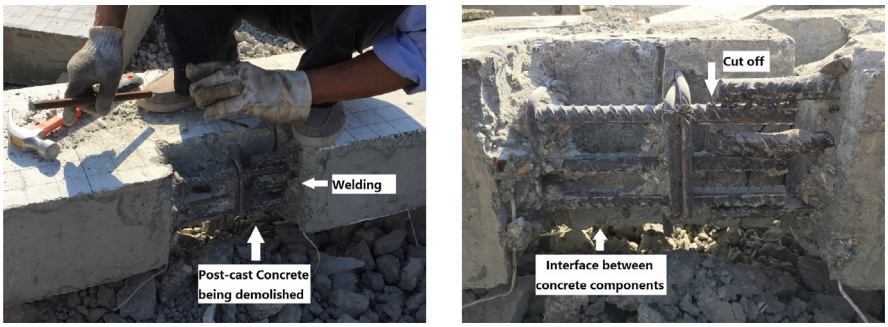

(a) Specimen during deconstruction (b) Bare reinforcement during deconstruction

Fig. 14. Deconstruction process after tests.

Based on the observation during the deconstruction process, suggestions are proposed to optimize the design of the DfD concrete connection like this kind of specimens in the future. The surface of the concrete component should be as smooth as possible before casting the concrete encasement. Suitable polish or thin-film can be adopted before concrete casting which will greatly reduce the difficulty of removing the encasing concrete. What is more important is that the length of the bare steel should be sufficient so that to achieve the reinforcement continuity during the reused process. Elaborate work should be carefully undertaken during the initial design procedure.

There are also some limitations of this study. The first is for the design, only one kind of DfD concrete connections was proposed in this research while there must be more connections that have DfD potential to be studied. Secondly, though the welded reinforcement enhanced the integrity of the specimens, it also brings the inconvenience while dismantling. Maybe some advanced rebar connection technique should be adopted in following new DfD concrete connections. Furthermore, only beam specimens were employed in the present study. Therefore, in order to fully understand the actual application of this kind of DfD concrete connection, the amount of performed tests on the structural behavior was insufficient, especially on those specimens after deconstruction and reconstruction, like concrete joints, concrete frames and so on. Thus, it is suggested that two-series experimental tests could be carried out to assess the whole structural behavior of the DfD concrete connection before deconstruction and after reconstruction. This work should be conducted in the future research.

6. Conclusion

In the present study, a moment-resisting DfD concrete connection for concrete frame joints is proposed and the design concept is described in details. Both the static and cyclic flexural loading tests have been undertaken in order to obtain a comprehensive understanding on its structural behavior. Based on the results of the present investigation, the following conclusions and recommendations can be drawn:

(1) The proposed moment-resisting concrete connection for frame joints was shown to be capable of providing adequate moment resistance, which was feasible as a replication of cast-in-place connection for frame structures in a seismic region. The test results confirmed that the proposed DfD specimens demonstrated favorable ductility behavior both under static loading and cyclic loadings.
(2) No significant difference on crack propagation and failure pattern were observed between the monolithic specimens and DfD specimens. The first flexural crack was appeared along the beam-end. After yielding of the main reinforcement, specimens were failed in flexure due to the crushing of the compression concrete at the beam-end for all the five specimens. For DfD specimens whether made of NAC or RAC, most of flexural cracks and diagonal cracks were formed at the protruding beam, and no obvious damage crack can be found on the DfD part, which met with the main purpose of the design. Relatively speaking, more cracks appeared on DfD RAC specimen, especially in the connection area.
(3) The introduction of welding for longitudinal tension reinforcement significantly improved the structural behavior of DfD concrete connections. Compared to reference specimens, similar cracks distribution, stiffness deterioration, energy dissipation and high initial flexural cracking moment capacity, ultimate moment capacity, ductility ratio were also observed in the DfD specimens.
(4) Since RAC was designed to have the same compressive strength and workability as the corresponding NAC in this study, there was no significant difference in the service load deflection between NAC and RAC beams with the same reinforcement. The ultimate load of RAC specimens can be relatively lower both for monolithic and DfD specimens but within a reasonable limit. Therefore, within the scope of this research, the utilization of RAC in DfD components is technically feasible.
(5) On account of the small amount of post-cast concrete, mechanical removal process was easy and very little debris was generated during the deconstruction stage. Little

damage was occurred on the DfD concrete part. Though the tests on the reconstructed specimens were not conducted in this study, the structural behavior of the proposed new ductile DfD concrete connection has been thoroughly investigated. Research is on-going and future investigation should pay more attention on the behavior of DfD concrete structures after reconstruction.

Acknowledgments

The authors wish to acknowledge the financial support from the Distinguished Young Scholars of China by National Natural Science Foundation of China (NSFC) (No: 51325802) and the joint research project between NSFC and PSF (No. 5161101205).

References

[1] Naik TR. Sustainability of concrete construction. Pract Periodical Struct Des Constr 2008;13(2):98–103.
[2] Topcu IB, Şengel S. Properties of concretes produced with waste concrete aggregate. Cem Concr Res 2004;34(8):1307–12.
[3] Poon CS, Shui ZH, Lam L, Kou SC. Influence of moisture states of natural and recycled aggregates on the slump and compressive strength of concrete. Cem Concr Res 2004;34(1):31–6.
[4] Xiao J, Li J, Zhang C. Mechanical properties of recycled aggregate concrete under uniaxial loading. Cem Concr Res 2005;35(6):1187–94.
[5] Evangelista L, De Brito J. Mechanical behaviour of concrete made with fine recycled concrete aggregates. Cement Concr Compos 2007;29(5):397–401.
[6] Akbarnezhad A, Ong KCG, Zhang MH, Tam CT, Foo TWJ. Microwave-assisted beneficiation of recycled concrete aggregates. Constr Build Mater 2011;25(8):3469–79.
[7] Xiao J, Sun Y, Falkner H. Seismic performance of frame structures with recycled aggregate concrete. Eng Struct 2006;28(1):1–8.
[8] Xiao J, Ding T, Pham TL. Seismic performance of precast recycled concrete frame structure. ACI Struct J 2015;112(4):515–24.
[9] Choi WC, Yun HD. Compressive behavior of reinforced concrete columns with recycled aggregate under uniaxial loading. Eng Struct 2012;41:285–93.
[10] Gonzalez VCL, Moriconi G. The influence of recycled concrete aggregates on the behavior of beam-column joints under cyclic loading. Eng Struct 2014;60:148–54.
[11] Parastesh H, Hajirasouliha I, Ramezani R. A new ductile moment-resisting connection for precast concrete frames in seismic regions: an experimental investigation. Eng Struct 2014;70:144–57.
[12] Yuksel E, Karadogan HF, Bal İE, Ilki A, Bal A, Inci P. Seismic behavior of two exterior beam–column connections made of normal-strength concrete developed for precast construction. Eng Struct 2015;99:157–72.
[13] Güngör A. Evaluation of connection types in design for disassembly (DFD) using analytic network process. Comput Ind Eng 2006;50(1):35–54.
[14] Akbarnezhad A, Ong KCG, Chandra LR. Economic and environmental assessment of deconstruction strategies using building information modeling. Autom Constr 2014;37:131–44.
[15] Kibert CJ, Chini AR. Overview of deconstruction in selected countries. CIB report, task group 39; 2000.
[16] Chini AR. Deconstruction and materials reuse: technology, economic, and policy. CIB report, task group 39; 2001.
[17] Addis W, Schouten J. Principles of design for deconstruction to facilitate reuse and recycling. London: CIRIA; 2004.
[18] Crowther P. Design for disassembly - themes and principles. Australia: RAIA/BDP Environment Design Guide; 2005.
[19] Tanaka Y, Murakoshi J. Reexamination of dowel behavior of steel bars embedded in concrete. ACI Struct J 2011;108(6):659–68.
[20] Vidjeapriya R, Jaya KP. Experimental study on two simple mechanical precast beam-column connections under reverse cyclic loading. J Perform Constr Facil 2012;27(4):402–14.
[21] Psycharis IN, Mouzakis HP. Shear resistance of pinned connections of precast members to monotonic and cyclic loading. Eng Struct 2012;41:413–27.
[22] Zoubek B, Isakovic T, Fahjan Y, Fischinger M. Cyclic failure analysis of the beam-to-column dowel connections in precast industrial buildings. Eng Struct 2013;52:179–91.
[23] Bournas DA, Negro P, Molina FJ. Pseudodynamic tests on a full-scale 3-storey precast concrete building: behavior of the mechanical connections and floor diaphragms. Eng Struct 2013;57:609–27.
[24] Englekirk RE. Development and testing of a ductile connector for assembling precast concrete beams and columns. PCI J 1995;39(2):36–51.
[25] Englekirk RE. An innovative design solution for precast prestressed concrete buildings in high seismic zones. PCI J 1996;41(4):44–53.
[26] Hawileh R, Tabatabai H, Rahman A, Amro A. Non-dimensional design procedures for precast, prestressed concrete hybrid frames. PCI J 2006;51(5):110–30.
[27] Ozden S, Ertas O. Behavior of unbonded, post-tensioned, precast concrete connections with different percentages of mild steel reinforcement. PCI J 2007;52(2):32–44.
[28] Metelli G, Riva P. Behaviour of a beam to column "dry" joint for precast concrete elements. In: Proceedings of 14th world conference on earthquake engineering; 2008. p. 1–8.
[29] Kulkarni SA, Li B, Yip WK. Finite element analysis of precast hybrid-steel concrete connections under cyclic loading. J Constr Steel Res 2008;64(2):190–201.
[30] Li B, Kulkarni SA, Leong CL. Seismic performance of precast hybrid-steel concrete connections. J Earthquake Eng 2009;13(5):667–89.
[31] Choi HK, Choi YC, Choi CS. Development and testing of precast concrete beam-to-column connections. Eng Struct 2013;56:1820–35.
[32] Yang KH, Oh MH, Kim MH, Lee HC. Flexural behavior of hybrid precast concrete beams with H-steel beams at both ends. Eng Struct 2010;32(9):2940–9.
[33] Korkmaz HH, Tankut T. Performance of a precast concrete beam-to-beam connection subject to reversed cyclic loading. Eng Struct 2005;27(9):1392–407.
[34] Khoo JH, Li B, Yip WK. Tests on precast concrete frames with connections constructed away from column faces. ACI Struct J 2006;103(1):18–27.
[35] Ong KCG, Lin ZS, Chandra LR, Tam CT, Pang SD. Experimental investigation of a DfD moment-resisting beam-column connection. Eng Struct 2013;56:1676–83.
[36] Fathifazl G, Abbas A, Razaqpur AG, Isgor OB, Fournier B, Foo S. New mixture proportioning method for concrete made with coarse recycled concrete aggregate. J Mater Civ Eng 2009;21(10):601–11.
[37] Tam VWY, Gao XF, Tam CM. Microstructural analysis of recycled aggregate concrete produced from two-stage mixing approach. Cem Concr Res 2005;35(6):1195–203.
[38] Tam VWY, Gao XF, Tam CM. Comparing performance of modified two-stage mixing approach for producing recycled aggregate concrete. Mag Concr Res 2006;58(7):477–84.
[39] Fathifazl G, Razaqpur AG, Isgor OB, Abbas A, Fournier B, Foo S. Flexural performance of steel-reinforced recycled concrete beams. ACI Struct J 2009;106(06):858–67.
[40] Ignjatović IS, Marinković SB, Mišković ZM, Savić AR. Flexural behavior of reinforced recycled aggregate concrete beams under short-term loading. Mater Struct 2013;46(6):1045–59.
[41] Park R, Paulay T. Reinforced concrete structures. John Wiley & Sons; 1975. 769 p..
[42] ACI Committee 318. Building code requirements for structural concrete (ACI 318-08) and commentary (ACI 318R-08). American Concrete Institute; 2008.